Combined effects of ENSO and PDO on Activity of Major Hurricanes in Eastern North Pacific

Chaoming Huang[1,2] · Hailong Liu[2] · Xidong Wang[1,3]· Juncheng Zuo[4] · Ruyun Wang[1]

[1] College of Oceanography, Hohai University, Nanjing 210098, China

[2] School of Oceanography, Shanghai Jiao Tong University, Shanghai 200240, China

[3]Southern Marine Science and Engineering Guangdong Laboratory (Zhuhai), Zhuhai 519080, China

[4] College of Marine Sciences, Shanghai Ocean University, Shanghai 201306, China

E-mail of corresponding author: hailong.liu@sjtu.edu.cn

Abstract

Major hurricanes (MHs) in the eastern North Pacific (ENP) in 1970-2018 were clustered into 3 categories with different quantity, intensity, lifetime, translation speed, track and large-scale environmental fields. MHs in all three clusters are more active in the Pacific Decadal Oscillation (PDO) warm phase than cold phase period. There are two clusters that their relationship with El Niño Southern Oscillation (ENSO) were modulated by PDO. The first cluster generates and develops in the open ocean and has an increasing trend of annual frequency, which is more active during El Niño years than during La Niña years in the PDO cold phase, but equally active in the PDO warm phase. The second cluster generates in the nearshore and translate rapidly into the ocean, which is more active during La Niña years than during El Niño years in the PDO warm phase, but equally active in the PDO cold phase. The PDO modulation mainly result from that MHs are obviously active during La Niña years in the PDO warm phase, which can be explained by local warming sea surface temperature, lower vertical wind shear, increasing vorticity and weakening sinking branch of circulation like Hadley cell. Therefore, PDO modulation cannot be ignored when predict the activity of tropical cyclone in ENP, especially for MHs that enters the open ocean and threat the islands such as the Hawaiian Islands.

Keywords Major Hurricanes · El Niño and Southern Oscillation · Pacific Decadal Oscillation· Cluster Analysis

1 Introduction

The eastern North Pacific (ENP) is one of the most active regions of tropical cyclones (TCs) in the world, just following the western North Pacific (WNP) in terms of the number of TCs (NTC) and accumulated cyclone energy (ACE). At the same time, genesis of TCs of per unit area and unit time in ENP is the most active in globe (Molinari et al. 2000a and 2000b) which often is related to easterly waves from Africa (Avila 1991; Avila and Pasch 1992) and Madden-Julian Oscillation (MJO, Molinari et al. 1997; Maloney and Hartmann 2000). TCs in the ENP can bring huge rain, wind and storm surge to west coast of Mexico and American, leading to a great threat for human's lives and property. Thus, study, understanding and prediction of TCs activity such as genesis, intensity, track and landfall in ENP can be necessary.

TCs activity in ENP is significantly connected with ENSO (Landsea 2000; Chu 2004). Firstly, ENSO can influence TC's frequency (Whitney and Hobgood 1997). The vertical wind shear (VWS) and TC's potential intensity (a measure of the instability of the ocean-atmosphere system; Bister and Emanuel 1998) become more contributive to TC generation in El Niño years (Camargo et al. 2007a). Secondly, there are more intense TCs in El Niño years (Gray and Sheaffer 1991; Raga et al. 2013), dues to the effect of dynamic and thermodynamic factors by single or synergy (Chan 2009). Such as sea surface temperature (SST) is more above-normal value and larger range, which can lead more convection and support more energy for TCs activity. Moreover, Balaguru et al. (2013) and Jin et al. (2014) also demonstrated that heat content in the upper-layer ocean is more connective to TCs than SST. Besides, winter El Niño can affect ENP TCs activity in several months later, which mainly is caused by the heat discharge of Equator ocean during the subsequent months. On the other hand, ENSO can also influence TCs activity location. During El Niño years the genesis location shift westward and

66 southward (Irwin and Davis 1999; Collins 2007; Collins et al. 2016; Lupo et al. 2008). Collins (2007)
67 find that NTC or ACE in western part of ENP (west of 116°W) is related to ENSO (Camargo et al.
68 2008), which affected by atmosphere thermodynamic processes (relative humidity (RH), SST, vertical
69 motions). However, eastern part of ENP (east of 116°W) is the most active region for TC genesis, with
70 a weak relationship with ENSO but not significant. It may be due to environmental conditions (e.g.,
71 SST, RH) reach a threshold value, which may make local variables effect become less important.
72 Although NTC in the central Pacific is small, including local generation and those which generate in
73 ENP and then move to central Pacific, ENSO can also influence the frequency of TCs in the central
74 Pacific due to the westward extend of monsoon trough, horizontal shear and vorticity of cyclone (Chu
75 and Wang 1997).
76 TCs in ENP are also associated with longer time scales variabilities like Pacific Decadal
77 Oscillation (PDO) (Martinez-Sanchez and Cavazos 2014; Lupo et al. 2008). Using bayesian multiple
78 change point analysis, Zhao and Chu (2006) find decadal variation with change points in around 1982
79 and 1998, showing active periods in 1982-1998 and inactive eras in 1972-1981 or 1999-2003. There are
80 more active TC years and more storms in PDO warm phase, especially for weaker storms. The effect of
81 PDO on TC activities was single or synergistic through oceanic and atmospheric variables (Lupo 2011),
82 which was similar to ENSO to some extent. Boucharel et al. (2016) analyzed 1980-2012 seasonal ACE
83 by empirical orthogonal functions analysis (EOF), indicating that the first two EOF modes are related
84 to not only eastern and central Pacific ENSO, but also PDO. Both PDO signal and PDO-ENSO
85 superposed signal affect interannual variation of TC frequency in ENP (Lupo et al. 2008). When
86 discussing ENSO effects under different phases of PDO, there are much more TCs during El Niño
87 years than during La Niña years in the warm phase of PDO, but less (fuzzy) difference in the cold

88 phase of PDO (Lupo 2011). However, previous studies have not separately discussed major hurricanes
89 (MHs, categories 3-5 in the Saffir–Simpson scale) (Saffir 1977; Simpson and Riehl 1981). When we
90 calculate the ACE of TCs in ENP in different categories (Table 1), we find that the ACE of MHs is
91 close to 70 percentage of all TCs. And ENSO and PDO are related with MHs significantly, but little
92 relation for weaker hurricanes. These results indicates that MHs may be the most important part to
93 discuss TCs activity in ENP. Thus, in this paper we focus on MHs and their relation with ENSO (PDO),
94 rather than weaker hurricanes.
95 In addition, Lupo (2011) divided ENP basin into four parts sub-basin by 20°N and 125°W
96 according to the SST status with a bit of subjective. They found that the two southern parts sub-basin
97 have significantly more hurricanes than northern sub-basins, and have more hurricanes in El Niño
98 years. Collins (2007) and Camargo et al. (2008) made a more reasonable partition by cluster analysis,
99 but they just carried out a comprehensive analysis between NTC (ACE or track) of hurricanes and
100 ENSO, without discussing the PDO modulation to this relationship. Therefore, this paper intends to
101 explore the interannual variation of MHs in different sub-basins in ENP by cluster analysis, especially
102 in different ENSO years combined with the PDO phase.
103 The rest of this paper is organized as follows. The data and method are introduced in section 2. The
104 activity of MHs in ENP in different ENSO-PDO phases is investigated by the cluster analysis in section
105 3. Interannual and decadal variability of MHs associated with ENSO and PDO is explored by EOF
106 analysis by ACE in section 4. The discussion and conclusion are given in section 5.
107

2 Data and methods

2.1 Data

The hurricanes data in ENP in 1970-2018 is HURDAT2, which comes from National Hurricanes Center (NHC) (Landsea and Franklin 2013). The data quality prior to 1970s is considered to be poorer because of the lack of satellite coverage and all hurricanes before that date were classified as a category one (e.g., Schultz 2007; Lupo 2011). Some of the weaker storms may be missing especially for the storms over the open ocean. 223 major hurricanes (MHs, in categories 3-5 hurricane) in 1970-2018 is selected in our work according to the Saffir–Simpson scale (Saffir 1977; Simpson and Riehl 1981).

The large-scale atmospheric environment variables are taken from the U.S. National Centers for Environmental Predication-National Center for Atmospheric Research (NCEP–NCAR) with a spatial resolution of 2.5°latitude×2.5°longitude and a time resolution of daily (Kalnay et al. 1996) from 1970 to 2018. Anomalies are defined relative to the climatology of the period in 1970-2018. Before analysis, we perform 3-day running means to obtain the data that remove the data's higher frequency information.

The monthly mean SST data comes from the Extended Reconstruction Sea Surface Temperature (ERSST) v5 (Huang et al. 2017) during the same period of 1970-2018, which comes from the National Climatic Data Center (NCDC), National Oceanic and Atmospheric Administration (NOAA). Anomaly are defined relative to the climatology of the period in 1970-2018. The Niño3.4 index is the average of SST anomaly calculated from the Niño3.4 area (5°S–5°N; 170°–120°W; Barnston et al. 1997). Same as Goddard and Dilley (2005) and Camargo et al. (2008), we define ENSO years according to the Niño3.4 index. First, we gain the annual Niño3.4 index by averaging over July to September (JAS), which are the peak months of the hurricane season in ENP. Then the 13 years (approximately 25% of the 49-year

period) with the largest or smallest values of annual Niño3.4 index in the period of 1970-2018 are defined as El Niño and La Niña years, respectively; the remaining 23 years are classified as neutral years. This percentile method corresponds to the Northern Hemisphere summers before the peaks of the ENSO events, and correspond well to the ENSO events obtained using more traditional definitions.

The PDO index is used to identify the PDO phases (warm or cold), which is defined as the leading principal component of monthly SST anomalies in the North Pacific Ocean poleward of 20°N (Mantua et al. 1997). We obtain PDO index from Physical Sciences Division (PSD) of Earth System Research Laboratory (ESRL) in NOAA (https://psl.noaa.gov/data/correlation/pdo.data). After performing a 10-year Gaussian filter, we obtain the multi-decadal variability of PDO, two cold phase periods with low PDO values: 1970-1976 and 1998-2013, and two warm phases period with high PDO values: 1977-1997 and 2014-2018, which basically consistent with previous studies (Zhang et al. 1997; Wang et al. 2009; Wang and Liu 2016).

The indices of North Atlantic Oscillation (NAO), Atlantic Meridional Mode (AMM) and Atlantic Multidecadal Oscillation (AMO) are downloaded from PSD in ERSL (https://psl.noaa.gov/data/climateindices/list/). Same as Niño3.4 index, we choose averaged value of PDO, Atlantic indices and all environment variables in JAS as the year value.

2.2 Method

Methods in this paper such as cluster analysis, composite analysis, empirical orthogonal functions (EOF) analysis, wavelet analysis, correlation and regression analysis are used. Cluster analysis classify the trajectories into several groups with different common features. In our study, we apply a technique that first developed by Gaffney et al. (2007) and widely used in previous studies (Camargo et al. 2007a,

2007b and 2008; Kossin et al. 2010; Mei and Xie 2016), to group TCs into different clusters based on the longitude and latitude of MH tracks (Gaffney and Smyth 1999, 2005; Gaffney 2004). The description of this technique parallels that of Camargo et al. (2007a and 2008), and Mei and Xie (2016). We model highly non-Gaussian densities based on the finite mixture model (Everitt and Hand 1981), and then extend the standard mixture modelling framework. Each cluster gains its own shape parameters by expectation maximization (EM) algorithm (DeSarbo and Cron 1988; Gaffney and Smyth 1999; McLachlan and Krishnan 1997; McLchlan and Peel 2000), and every trajectory is assumed to be generated by one of K (K=3 in this study) different regression models that have the highest posterior probability. More details about this cluster method can be found in Gaffney 2004 and Camargo et al. (2007a and 2008).

3 Cluster analysis of major hurricanes

3.1 Cluster characteristics of major hurricanes

MHs that occur in different regions will have different number, energy and movement characteristics, as well as different environmental variable characteristics. Collins and Mason (2000) found that environmental parameters affecting TCs activity are different in east and west of 116°W. Therefore, it is necessary to divide the ENP basin into several sub-basins for MHs analysis. Here we use the clustering method to separate MH tracks into 3 groups, which is same as Camargo et al. (2008). Here, the cluster number K selected as 3 can make the clustering analysis have a better fitting effect.

Basic characteristics of three clusters are shown in Fig. 1 and Table 2. Cluster A is active in the open ocean far away from the shore with the main activity region in 182.7-227.5°E, 11.8-23.6°N. Cluster B is generated near the shore and moves into the open ocean with the main activity region in

213.4-245.0°E, 13.4-19.5°N. Besides, cluster B shows the fastest translation speed, the longest average track length, but not the longest lifetime. Cluster C is active near the shore area, and their trajectories are mostly parallel to the coastline with the main activity region in 240.4-256.0°E, 13.4-21.2°N. These three clusters are roughly arranged in an east-west distribution, and with westward-northwestward movement. The closer to the coast, the more northward the average genesis location shifts. The number of cluster C accounted for 54.26% of the total MHs, and its ACE accounted for 48.52%, indicating that the average ACE per MH is slightly small. It may be because cluster C is nearshore, with a higher probability of landing, reducing the intensity and life cycle. The active peak months of these three clusters are different. Cluster B reaches its most active time in July firstly, followed by cluster A peaking in August, and cluster C peaking in September.

The condition of the large-scale environmental field cannot be ignored for the activity of MHs. For example, steering flow (SF) will affect the direction and translation speed of MHs, and VWS will affect the generation, strength and track of MHs. Therefore, we used the wind field data from NCEP reanalysis dataset to gain SF fields which is calculated as the function of $\frac{\int_{100}^{1000}\vec{V}dp}{\int_{100}^{1000}dp}$ (Anthony Reynes 2003). It can be seen from the vector in Fig. 2 that the composites of the SF are significant in almost all the field. Each cluster's mean regression curve has a good consistency with SF, which has a stronger zonal component than meridional component, making MHs more westward-northwestward movement. Cluster B has the most obvious and strongest northwestward SF, which makes cluster B move fastest among three clusters. At the same time, VWS between 850 and 200-hPa is also an important factor for the TC activity. VWS is mainly distributed with zonal strips. VWS over the most of the 10°S-10°N in the equatorial region is negative, expanding poleward along the eastern coastline of American and Mexico. There is a high value of VWS extending from the continent of United States to the southwest.

196 MHs are mostly generated and act in the low value of VWS. Moreover, SST and atmospheric 850-hPa
197 wind vorticity are also important environmental factors to affect TCs activities. We show the
198 composites of SST and 850-hPa wind anomaly of each cluster and all MHs in Fig. 3. SST anomaly
199 shows the patterns of El Niño events, especial in cluster A, which is similar to Camargo et al. (2008).
200 MHs usually occur the area that above-normal SST. Besides, there is a positive vorticity that almost
201 covers the entire region of MHs activity of three clusters, indicating that the vorticity of the 850-hPa
202 wind has a significant impact on MHs activity of the ENP, especially for intensity.
203
204 **3.2 Effect of different ENSO and PDO phases on activity of major hurricanes in each cluster**
205 The annual number of MHs (NMH) and ACE of MHs is significantly correlated with ENSO and
206 PDO (Table 1). We calculated the mean NMH or ACE per year of each cluster in different ENSO or
207 PDO phase years and the combination phases of ENSO and PDO (Fig. 4). In the warm phase of PDO,
208 the number and ACE of all MHs are higher than those in the cold phase of PDO. However, the
209 relationship of two clusters with ENSO is modulated by PDO. Cluster A has significantly more NMH
210 and ACE during El Niño years than during La Niña years in the PDO cold phase, but less difference or
211 equally active in the PDO warm phase (Figs. 4a, 4b). Cluster B is more active during La Niña years
212 than during El Niño years in the warm PDO phase, but equally active in the PDO cold phase (Figs. 4c,
213 4d). These PDO modulation mainly result from that MHs are obviously active during La Niña years in
214 the PDO warm phase. Cluster C is more active during El Niño years than during La Niña years in the
215 both PDO cold and warm phases (Figs. 4e, 4f), indicating that the relationship between cluster C and
216 ENSO is less affected by the PDO.
217 Furthermore, we calculate the composite differences of ACE distribution of each cluster between

PDO warm and cold phase, between El Niño and La Niña years in the different PDO phases (Fig. 5). The ACE is distributed on a 2°latitude×2°longitude grid same as EOF analysis in the next section. It is basically consistent with the results of Fig. 4. All three clusters are more active in the PDO warm than cold phase (Figs. 5a, 5d, 5g). The composite differences between El Niño and La Niña years of clusters A and B vary with the PDO phase shift (Figs. 5b, 5c, 5e, 5f). For cluster A, the difference is larger in the PDO warm phase than PDO cold phase (Figs. 5b, 5c), but in the PDO warm phase the area is almost equally for positive and negative value, positive value in the north or west and negative value in the south or east, cause less difference between El Niño and La Niña years, compared with that the range of positive value is obviously larger than that negative value in the PDO cold phase. For cluster B, it is more active during La Niña years than during El Niño years around 110°W-150°W and 15°N-25°N in the warm PDO phase (Fig. 5e), but equally active in the PDO cold phase (Fig. 5f). Cluster C had larger value of composite differences during El Niño years in both PDO warm and cold phase (Figs. 5h, 5i), but the location of positive value is slightly different between the cold and warm phase of PDO, it is southerly in the warm phase of PDO, and northerly in the cold phase of PDO. At the same time, the composite difference maps of track density are basically the similar with ACE distribution. Therefore, it can be basically concluded that the relationships of the mean NMH (ACE) per year, track (ACE) density with ENSO are modulated by the phase change of PDO in clusters A and B. However, the relationship of the mean NMH (ACE) per year and ENSO is basically not modulated by the phase change of PDO in cluster C, but the spatial pattern of track and ACE density is slightly different in the cold and warm phase of PDO.

TC activity is obviously related to the environmental variables and circulations. Thus, we investigate the environmental variables in different phase of ENSO and PDO. Composite differences of

240 SST anomaly (SSTA) and VWS are shown in Fig. 6. Compared with those in the PDO clod phase,
241 VWS is much lower and SST is much higher over the developing area of west of 120°W and north of
242 15°N, which contributes to more MHs genesis and development in the PDO warm phase. By the same
243 way, composite differences of zonal and meridional circulation of main activity region of MHs in ENP
244 can be given in Fig. 7. We can find significant ascending branch in most part of activity region of MHs,
245 except for zonal circulation of main activity region for cluster C, indicating that the atmospheric and
246 oceanic conditions are more conducive to MHs activity in the PDO warm phase.
247 Like the analysis of environmental factors in the warm and cold phase of PDO, we also show the
248 composite differences of SST and VWS between El Niño and La Niña years for the PDO warm phase
249 and PDO cold phase period (Fig. 6). Besides, we calculate annual mean of VWS, vorticity anomaly in
250 850-hPa and SST anomaly in the main activity region of each cluster in different ENSO and PDO
251 phases, in order to quantify the difference of each variable and their contributions to every cluster (Fig.
252 8). Further, we use local meridional and zonal circulations of each cluster to explain the variability of
253 environmental factors in the different PDO phase (Figs. 9-11).
254 For cluster A, it is much warmer SST during El Niño years than La Niña years in the PDO cold
255 phase (Fig. 6e) in main activity region of cluster A, but less difference in PDO warm phase (Fig. 6c and
256 Fig. 8c), which matches the active characteristics of cluster A (Fig. 4 and Fig. 5). Secondly, higher
257 vorticity during La Niña years in the PDO warm phase (Fig. 8b) also makes more MHs form at that
258 time. The difference of MH activity, SST, and vorticity can be explained from the meridional
259 circulation over the main activity region of cluster A (red dotted box in Fig. 9). In the meridional
260 circulation of main activity region for cluster A (Figs. 9a, 9b), a larger ascending flow often is
261 accompanied by warmer SST and higher vorticity in the PDO cold phase, rather than in the PDO warm

phase in the middle troposphere (Fig. 9b). In the lower troposphere (Figs. 9a, 9b), northward wind can bring warm sea water from tropical region in the PDO cold phase, but without this northward wind in the PDO warm phase. However, we could not find this PDO modulation in the zonal circulation (Figs. 9c, 9d). The ascending flow in the middle troposphere and sinking flow on the east part of lower troposphere (around 140°W) in main activity region of the cluster A (red dotted box)， which offsets each other and therefore reduce the difference in vertical motion in the PDO warm phase (Fig. 9c). Meantime, there are also little difference of vertical motion in the PDO cold phase (Fig. 9d).

Compared with in the PDO cold phase, the smaller VWS and larger vorticity during La Niña years than El Niño years in main activity region of cluster B (Figs. 6d, 6f, 8a, 8b) contribute to the active MHs during La Niña years in the PDO warm phase (Fig. 4 and Fig. 5). In the composite differences of zonal circulation in cluster B main activity region (blue dotted box in Figs. 10c, 10d), more obvious sinking flow in lower and middle troposphere of in the PDO warm phase represent a larger vorticity during La Niña years in the PDO warm phase. Besides, larger value of VWS in the PDO warm phase can also find in the zonal circulation. The meridional circulation shows less significant differences than zonal circulation in Figs. 10a and 10b, with both ascending and sinking flow in the main activity region of cluster B (blue dotted box) resulting in no consistent vertical movement. It may be result from the narrow east-west stripe track shape of cluster B.

Differences between El Niño years and La Niña years of environmental factors and circulations in cluster C is similar in the both PDO warm and cold phase, indicating that PDO less modulate the relationship of ENSO and cluster C (Figs. 6, 8 and 11).

4 Interannual and decadal EOF analysis of ACE for major hurricanes

In order to confirm the results of Cluster analysis MHs activity depend on the different regions, we choose another way (EOF analysis) to analyze the interannual and decadal variability of MH activity like Boucharel et al. 2016. First of all, we construct annual ACE-gridded data. We sum from Jan to Dec as the annual value for each MH's ACE over the total period of 1970-2018 at a 2°latitude×2°longitude spatial resolution, and then average in a 6°×6° sliding domain over the whole ENP to reduce the noise level. The linear trend pattern of MHs ACE were showed in Fig. 12a and four periods of different phase of PDO can also be obtained (without shown here). The ENP basin showed the increase-decrease-increase trend pattern from west to east, but most of the basin (coastal area and open ocean) have the increase trend, which indicates that more MHs appears in areas far from the mainland and landfalls. In addition, after inspecting the time series of the annual NMH (Fig. 1h), there is slight increase trend, especially for cluster A in Fig. 1a. The range of this increase trend is westward shift in the warm phase of PDO. Besides, trend of track density shows similar phenomena (Fig. 12b).

After preliminary checking the MHs trend pattern in ENP, we further explored the interannual and decadal variability of ACE by EOF analysis. Before that, we detrend the annual ACE gridded data to reduce signal interference on a longer time scale, such as global warming. At the same time, PDO index and environmental atmospheric variables were averaged from July to September (JAS), because July to September is the peak season of MHs in the ENP (same as Camargo et al. 2008) that approximately 75% of the number (or ACE) of all MHs. But when discuss the interannual variability of ACE, Nino3.4 index and SST were averaged over May to Jul (or Jan to Mar) before JAS because of the delayed effect of the ENSO oceanic state on TC in ENP (Boucharel et al. 2016).

304 **4.1 Interannual EOF analysis of ACE**

305 In order to better identify ENSO and PDO signals in MHs, we perform filter processing (zero-
306 phase bandpass filter) for annual ACE to obtain ACE signals of 2-7 years and longer than 7 years
307 before EOF analysis. The first two modes of EOF analysis of 2-7 years bandpass filtered of ACE are
308 shown in Fig. 13, which can explain 31.6% and 13.5% of the variance. Their time series or principal
309 component (PC) shows a significant correlation with pre-Niño3.4 index (May-Jul for PC1 and Jan-Mar
310 for PC2), which is similar to Boucharel et al. (2016).

311 Besides, the series of 10-year sliding correlations between normalized PC1 and Niño3.4 index is
312 significant connected to PDO. The correlation coefficients are larger and more significant in the cold
313 phases of PDO than in the warm phases of PDO. The spatial mode of EOF1 shows positive value in the
314 10-20°N and 100-125°W, which basically cover the mean regression curves of three clusters in
315 previous section. The relation of ENSO and MHs, and PDO modulation can be identified again by EOF
316 analysis. Cluster A (B, C) is equally (less, more) activity during El Niño years than La Niña years in the
317 PDO warm phase that make the little relation after combining the relations of three clusters and ENSO.
318 However, cluster A (B, C) is more (equally, more) activity during El Niño years than La Niña years in
319 the PDO cold phase, that it has a significantly positive running relation with ENSO after combining the
320 relations of three clusters and ENSO. The second EOF mode has a dipole spatial pattern but lower
321 variance, and its running relation with ENSO is not significant.

322 The relationship between MHs and ENSO also can be found in environmental factors. The
323 regressions of SST anomaly, 850-hPa wind anomaly, SF, and VWS onto PC1 show the relationships
324 between several environmental variables and the first dominant mode (Fig. 14). The relationship
325 between VWS or SST anomaly with the first mode is obvious, but the correlation with local SF and

850-hPa wind anomaly is slightly weaker. Patterns of these variables basically show the characteristics associated with El Niño event, such as the warming of SST in the equatorial eastern Pacific, westerly winds in the equatorial western Pacific, and equatorial low VWS. From the regression patterns in different PDO phases, we can find local SF, VWS and SST have a better relation with PC1 in the PDO cold phase than in PDO warm phase. The third and fourth EOF modes explain only 12.2% and 6.8% of the variance, but their PCs are not correlated with Nino3.4 index, and regressions of environmental variables on PCs are not significant.

4.2 Decadal EOF analysis of ACE

The first EOF mode of decadal signal of ACE density is shown in Fig. 15, which explains 52.5% of the variance. Its spatial mode is similar to the first EOF mode of interannual signal in Fig. 14, but the range of positive value extends westward. The PC1 is significantly correlated with the PDO index, with a correlation coefficient of 0.6. It also indicates that the influence of PDO on MHs includes modulation of the relationship between MHs and ENSO, as well as its direct effect on MHs. The regressions of environmental variables onto PC1 are also very similar to the composite differences between PDO warm and cold phase (Figs. 6a, 6b) that is conducive to MHs activities in PDO warm phase. The second, third, and fourth EOF modes explain only 15.5%, 9.7%, and 5.9% of the variance, and their PCs are not correlated with PDO. Besides, regressions of environmental variables onto their PCs are not significant, indicating that decadal variability of ACE of MHs is highly relation to PDO, and only in the first EOF mode.

5 Discussion and conclusion

This paper analysis the activity of MHs in ENP by two different views, the Lagrangian thought (cluster analysis) and Euler thought (EOF analysis). MHs in the ENP were clustered into 3 categories. Cluster A is active in the open ocean far away from the shore and has an increasing trend of annual frequency, cluster B is generated near the shore and moves into the ocean with the fastest translation speed and the largest northwest SF, and cluster C is mainly active near the shore area that has the smallest mean ACE per MH but accounts for 54.26% of the total number of MHs. The active peak months of these three clusters is in July-September. The composites of the SF have a good consistency with these cluster's mean regression curve, which have a larger zonal component than meridional component, making MHs more west-northwestward movement. MHs are mostly generated and activity in the low value of VWS. SST anomaly in cluster A is obviously correlated with El Niño event, but less linked to El Niño event for clusters B and C. The annual NMH and ACE of MHs is significantly correlated with ENSO and PDO. MHs in the entire ENP basin has a more activity in the warm phase of PDO warm than cold phase. It is interesting that PDO only modulates the relationship of ENSO and MHs activity in clusters A and B. Cluster A is more active during El Niño years than during La Niña years in the PDO cold phase, but equally active in the warm PDO phase. Cluster B is more active during La Niña years than during El Niño years in the warm PDO phase, but equally active in the PDO cold phase. These differences of PDO modulation for the two clusters may be because MH is obviously active during La Niña years in the PDO warm phase, which can be explained by local warming SST (for cluster A), lower VWS (for cluster B), increasing vorticity (for clusters A and B) and different vertical motions in the meridional circulation (for clusters A) and zonal circulation (for cluster B). The results indicate that PDO modulates MHs in different regions through different environmental

369 variables. However, the relationship between cluster C and ENSO is almost unaffected by PDO.

370 The first EOF mode of decadal signal of ACE explains 52.5% of the variance, which is
371 significantly correlated with the PDO. The first EOF mode of interannual of ACE density shows a
372 significant correlation with ENSO, which is significantly modulated by PDO, with stronger relationship
373 with ENSO in the cold phase of PDO (1998-2014). Moreover, patterns of environmental variables
374 basically show the characteristics of the El Niño event, such as the warming of SST in the equatorial
375 eastern Pacific, westerly winds in the equatorial western Pacific, and equatorial low VWS.
376 Environmental variables also show a stronger relationship in PDO cold phase. The results also
377 consistent with in cluster analysis. The spatial mode covers the tracks of three clusters in section 3.
378 Cluster A (B, C) is equally (less, more) activity during El Niño years than La Niña years in the PDO
379 warm phase that make the little relation after combining the relations of three clusters and ENSO, but
380 cluster A (B, C) is more (equally, more) activity during El Niño years than La Niña years in the PDO
381 cold phase that it has the significantly positive relation with ENSO after combining the relations of
382 three clusters and ENSO. Our work highlights the combined effect of ENSO and PDO on TCs in ENP,
383 especial for MHs, which may have an important implication to climate prediction for ENP TC activity.

384 In fact, interannual variability of MHs in ENP is affected by not only Pacific climate variability
385 (ENSO or PDO), but also the Atlantic climate variabilities (e.g., Wang and Lee 2009; Raga et al. 2013;
386 Caron et al. 2015). After all, the ENP and the Atlantic are only separated by the long and narrow
387 Central America, their climates have obvious correlation, such as the seesaw phenomenon. The
388 influence of the Atlantic Ocean on the ENP is mainly through dynamic conditions (Caron et al. 2015),
389 such as VWS and convective instability (Wang and Lee 2009; Collins 2010). A series of climate factors
390 in Atlantic were choose as the predictors of TC activities in ENP, such as AMM, NAO and so on

(Caron et al. 2015). Raga et al. (2013) also showed that the main signal of the TC landing in Mexico from 1850 to 2010 was PDO, followed by ENSO and NAO, and NAO affected the TC landing. Therefore, we calculated correlation coefficients of JAS NAO, AMM and AMO indices and annual NMH (ACE). We find that the cluster C is significantly correlated with AMM, and only weak correlation with AMO. There is a weak correlation between cluster A and AMM. Regression of annual ACE and track density in each grid of cluster A, cluster B and cluster C onto normalized JAS AMM, AMO and NAO indices have different correlations in different regions (without shown here). Cluster A is negatively correlated with AMM and NAO in the total MHs activity area. Cluster B is negatively correlated with AMM in the western part of the activity area, positively correlated with NAO in the southwest part of the activity area. Cluster C is negatively correlated with AMM and AMO index in the main activity area, but positive relationship between cluster C and NAO index. Above results indicate that effects of Atlantic climate on ENP TC activity depend on the region, which need further investigate in the future study.

Acknowledgments

This work is supported by the National Key Research and Development Program of China 2016YFA0601804, Open Financial Grant from Qingdao National Laboratory for Marine Science and Technology QNLM2016ORP0101, Shanghai Typhoon Research Foundation, National Science Foundation of China 41776019 and HKUST-SJTU Joint Research Collaboration Fund. Chaoming Huang is supported by the National Key Research and Development Program of China 2016YFC1401905. We thank Scott J. Gaffney for providing the Matlab toolbox with the clustering algorithms described in his PhD paper at http://www.datalab.uci.edu/resources/CCT. NOAA ERSST V5 data are provided by the NOAA/OAR/ESRL PSD, Boulder, Colorado, USA at https://www.esrl.noaa.gov/psd/.

415

416 **References**

417 Anthony Reynes (2003) Environmental steering flow analysis for central north Pacific tropical

418 cyclones based on NCEP_NCAR reanalysis data. Ph.D. thesis, University of Hawaii

419 Avila LA (1991) Atlantic tropical systems of 1990. Mon Weather Rev 119:2027–2033.

420 doi:10.1175/1520-0493(1991)1192.0.CO;2

421 Avila LA, Pasch RJ (1992) Atlantic tropical systems of 1991. Mon Weather Rev 120:2688–2696

422 Balaguru KL, Ruby Leung, Yoon J-H (2013) Oceanic control of Northeast Pacific hurricane activity at

423 interannual timescales. Environmental Research Letters 8(4):044009. doi:10.1088/1748-

424 9326/8/4/044009

425 Barnston AG, Chelliah M, Goldenberg SB (1997) Documentation of a highly ENSO-related SST region

426 in the equatorial Pacific. Atmosphere Ocean 35:367–383. doi:10.1080/07055900.1997.9649597

427 Bister M, Emanuel KA (1998) Dissipative heating and hurricane intensity. Meteorology and

428 Atmospheric Physics 65(3–4):233–240. doi:10.1007/BF01030791

429 Boucharel J, Jin F-F, England MH, Lin I-I (2016) Modes of hurricane activity variability in the eastern

430 Pacific: Implications for the 2016 season. Geophys Res Lett 43:11358–11366.

431 doi:10.1002/2016GL070847

432 Camargo SJ, Emanuel KA, Sobel AH (2007a) Use of a Genesis Potential Index to Diagnose ENSO

433 Effects on Tropical Cyclone Genesis. J Clim 20(19):4819–4834. doi:10.1175/JCLI4282.1

434 Camargo SJ, Robertson AW, Gaffney SJ et al (2007b) Cluster Analysis of Typhoon Tracks. Part II:

435 Large-Scale Circulation and ENSO. J Clim 20(14):3654–3676. doi:10.1175/JCLI4203.1

436 Camargo SJ, Robertson AW, Barnston AG et al (2008) Clustering of eastern North Pacific tropical

437 cyclone tracks: ENSO and MJO effects. Geochemistry, Geophysics, Geosystems 9(6): Q06V05.
438 doi:10.1029/2007GC001861
439 Caron LP, Boudreault M, Camargo SJ (2015) On the Variability and Predictability of Eastern Pacific
440 Tropical Cyclone Activity*. J Clim 28(24):9678–9696. doi:10.1175/JCLI-D-15-0377.1
441 Chan JCL (2009) Thermodynamic control on the climate of intense tropical cyclones. Proceedings of
442 the Royal Society A 465:3011–3021. https://doi.org/10.1098/rspa.2009.0114
443 Chu PS (2004) ENSO and tropical cyclone activity, in Hurricanes and Typhoons: Past, Present and
444 Future, edited by R. J. Murnane and K.-B. Liu, pp. 297–332, Columbia Univ. Press, New York
445 Chu PS, Wang J (1997) Tropical cyclone occurrences in the vicinity of Hawaii: Are the differences
446 between El Niño and non-El Niño years significant? J Clim 10:2683–2689.
447 https://doi.org/10.1175/1520-0442(1997)010<2683:TCOITV>2.0.CO;2
448 Collins J (2010) Contrasting High North-East Pacific Tropical Cyclone Activity with Low North
449 Atlantic Activity. Southeastern Geographer 50(1):83–98. doi:10.1353/sgo.0.0069
450 Collins JM (2007) The Relationship of ENSO and Relative Humidity to Interannual Variations of
451 Hurricane Frequency in the North-East Pacific Ocean. Auckland University of Technology, 98(6):
452 110. doi:10.1094/PHYTO-98-6-0743
453 Collins JM, Mason IM (2000) Local environmental conditions related to seasonal tropical cyclone
454 activity in the Northeast Pacific basin. Geophys Res Lett 27:3881–84. doi:10.1029/2000GL011614
455 Collins JM, Klotzbach PJ, Maue RN, Roache DR, Blake ES, Paxton CH, Mehta CA (2016) The record-
456 breaking 2015 hurricane season in the eastern North Pacific: An analysis of environmental
457 conditions. Geophys Res Lett 43:9217–9224. doi:10.1002/2016GL070597
458 DeSarbo WS, Cron WL (1988) A maximum likelihood methodology for clusterwise linear regression.

459 Journal of Classification 5(2):249–282. doi:10.1007/BF01897167

460 Everitt BS, Hand DJ (1981) Finite Mixture Distributions. The Mathematical Gazette 77(379).

461 doi:10.1002/0471715816.ch8

462 Gaffney SJ, Smyth P (1999) Trajectory clustering with mixture of regression models. In Proceedings of

463 the fifth ACM SIGKDD international conference on Knowledge discovery and data mining (KDD

464 '99). Association for Computing Machinery, New York, NY, USA, 63–72.

465 https://doi.org/10.1145/312129.312198

466 Gaffney SJ (2004) Probabilistic curve-aligned clustering and prediction with regression mixture

467 models. Ph.D. thesis, University of California, Irvine, CA

468 Gaffney SJ, Smyth P (2005) Joint probabilistic curve-clustering and alignment. Advances in Neural

469 Information Processing Systems 17: Proceedings of the 2004 Conference, L. K. Saul, Y. Weiss,

470 and L. Bottou, Eds., MIT Press, 473–580

471 Gaffney SJ, Robertson AW, Smyth P et al (2007) Probabilistic clustering of extratropical cyclones using

472 regression mixture models. Clim Dyn 29(4):423–440. doi:10.1007/s00382-007-0235-z

473 Goddard L, Dilley M (2005) El Niño: Catastrophe or opportunity? J Clim 18(5):651–665.

474 doi:10.1175/JCLI-3277.1

475 Gray WM, Sheaffer JD (1991) El Niño and QBO influences on tropical cyclone activity, in

476 Teleconnections Linking Worldwide Anomalies, edited by M. H. Glantz, R. W. Katz, and N.

477 Nicholls, pp. 257–284, Cambridge Univ. Press, New York.

478 Huang B, Thorne PW, Banzon VF, Boyer T, Chepurin G, Lawrimore JH, Menne MJ, Smith TM, Vose

479 RS, and Zhang H-M (2017) NOAA Extended Reconstructed Sea Surface Temperature (ERSST),

480 Version 5. [indicate subset used]. NOAA National Centers for Environmental Information.

481 doi:10.7289/V5T72FNM [access date].
482 Irwin RP, and Davis RE (1999) The relationship between the Southern Oscillation Index and tropical
483 cyclone tracks in the eastern North Pacific. Geophys Res Lett 26(15):2251–2254.
484 doi:10.1029/1999GL900533
485 Jin F-F, Boucharel J, Lin I-I (2014) Eastern Pacific tropical cyclones intensified by El Niño delivery of
486 subsurface ocean heat. Nature 516(7529):82–85. doi:10.1038/nature13958
487 Kalnay et al (1996) The NCEP/NCAR 40-year reanalysis project. Bulletin of the American
488 Meteorological Society 77(3):437–472. doi:10.1175/1520-
489 0477(1996)077<0437:TNYRP>2.0.CO;2
490 Kossin JP, Camargo SJ, Sitkowski M (2010) Climate Modulation of North Atlantic Hurricane Tracks. J
491 Clim 23(11):3057–3076. doi:10.1175/2010JCLI3497.1
492 Landsea CW (2000) El Niño–Southern Oscillation and the seasonal predictability of tropical cyclones,
493 in El Niño: Impacts of Multiscale Variability on Natural Ecosystems and Society, edited by H. F.
494 Dı´az and V. Markgraf, pp. 149–181, Cambridge Univ. Press, New York
495 Landsea CW, Franklin JL (2013) Atlantic Hurricane Database Uncertainty and Presentation of a New
496 Database Format. Mon Weather Rev 141:3576–3592. doi:10.1175/MWR-D-12-00254.1
497 Lupo AR (2011) The Interannual and Interdecadal Variability in Hurricane Activity. Recent Hurricane
498 Research – Climate, Dynamics and Societal Impacts, IntechOpen. doi:10.5772/14598
499 Lupo AR, Latham TK, Magill TH, Clark JV, Melick CJ, Market PS (2008) The Interannual Variability
500 of Hurricane Activity in the Atlantic and East Pacific Regions. National Weather Digest 32(1):11–
501 33
502 Maloney ED, Hartmann DL (2000) Modulation of hurricane activity in the Gulf of Mexico by the

503 Madden-Julian oscillation. Science 287:2002–2004. doi:10.1126/science.287.5460.2002
504 Mantua NJ, Hare SR, Zhang Y, Wallace JM, Francis RC (1997) A Pacific interdecadal climate
505 oscillation with impacts on salmon production. Bulletin of the American Meteorological Society
506 78:1069–1079. doi:10.1175/1520-0477(1997)078<1069:APICOW>2.0.CO;2
507 Martinez-Sanchez J, Cavazos T (2014) Eastern Tropical Pacific hurricane variability and landfalls on
508 Mexican coasts. Climate Research 58(3):221–234. doi:10.3354/cr01192
509 McLachlan, Krishnan T (1997) The EM Algorithm and Extensions. John Wiley and Sons, 274 pp.
510 McLachlan, Peel D (2000) Finite Mixture Models. John Wiley and Sons, 419 pp.
511 Mei W, Xie S-P (2016) Intensification of landfalling typhoons over the northwest Pacific since the late
512 1970s. Nature Geoscience 9(10):753–757. https://doi.org/10.1038/ngeo2792
513 Molinari J, Knight D, Dickinson M, Vollaro D, Skubis S (1997) Potential vorticity, easterly waves, and
514 eastern Pacific tropical cyclogenesis. Mon Weather Rev 125:2699–2708.
515 https://doi.org/10.1175/1520-0493(1997)125<2699:PVEWAE>2.0.CO;2
516 Molinari J, Vollaro D (2000a) Planetary- and synoptic-scale influences on eastern Pacific cyclogenesis.
517 Mon Weather Rev 128:3296–3307. doi:10.1175/1520-0493(2000)128<3296:PASSIO>2.0.CO;2
518 Molinari J, Vollaro D, Skubis S, Dickinson M (2000b) Origins and mechanisms of eastern Pacific
519 tropical cyclogenesis: A case study. Mon Weather Rev 128:125–139. doi:10.1175/1520-
520 0493(2000)128<0125:OAMOEP>2.0.CO;2
521 Raga GB, Bracamontes-Ceballos B, Farfan LM, Romero-Centeno R (2013) Landfalling tropical
522 cyclones on the Pacific coast of Mexico: 1850-2010. Atmosfera 26(2):209–220.
523 doi:10.1016/S0187-6236(13)71072-5
524 Saffir HS (1977) Design and construction requirements for hurricane resistant construction. ASCE

525 Tech. Rep. Preprint 2830, 20 pp.

526 Schultz LW (2007) Some climatological aspects of tropical cyclones in the eastern north Pacific.

527 National Weather Digest 32(1):45–54

528 Simpson RH, Riehl H (1981) The Hurricane and Its Impact. Louisiana State University Press, 398 pp.

529 Wang C, Lee S-K (2009) Co-variability of tropical cyclones in the North Atlantic and the eastern North

530 Pacific. Geophys Res Lett 36(24):L24702. doi:10.1029/2009GL041469

531 Wang X, Liu H (2016) PDO modulation of ENSO effect on tropical cyclone rapid intensification in the

532 western North Pacific. Clim Dyn 46(1–2):15–28. doi:10.1007/s00382-015-2563-8

533 Wang X, Wang D, Zhou W (2009) Decadal variability of twentieth century El Niño and La Niña

534 occurrence from observations and IPCC AR4 coupled models. Geophys Res Lett 36:L11701.

535 doi:10.1029/2009GL037929

536 Whitney LD, Hobgood J (1997) The relationship between sea surface temperature and maximum

537 intensities of tropical cyclones in the eastern North Pacific. J Clim 10:2921–2930.

538 doi:10.1175/1520-0442(1997)010<2921:TRBSST>2.0.CO;2

539 Zhang Y, Wallace JM, Battisti DS (1997) ENSO-like Interdecadal Variability: 1900–93. J Clim

540 10(5):1004–1020. doi:10.1175/1520-0442(1997)010<1004:ELIV>2.0.CO;2

541 Zhao X, Chu P-S (2006) Bayesian multiple changepoint analysis of hurricane activity in the eastern

542 North Pacific: A Markov chain Monte Carlo approach. J Clim 19:564–578.

543 doi:10.1175/JCLI3628.1

544

545

546

Tables

Table 1 Mean NTC/ACE per year of different intensity scales of TCs in 1970-2018 in ENP, percent values represent the proportions within all TCs. And correlation coefficients of JAS Niño3.4 (PDO) indices and annual NTC (ACE), the correlation coefficient is marked the 90% significant in boldface, and 95% significant is denoted with an asterisk (*). One ACE equals to 10000 kt^2 (kn^2).

Features of TCs	TD	TS	Cat1-2	Cat3-5	All TCs
Mean NTC per year and percentage	2.00 / 10.69%	7.32 / 39.15%	4.84 / 25.84%	4.55 / 24.32%	18.71 / 100%
Mean ACE per year and percentage	--	12.66 / 9.12%	34.13 / 24.58%	92.06 / 66.30%	138.85 / 100%
Correlation of annual NTC and JAS Niño3.4 index	0.01	0.17	0.03	**0.35***	**0.32***
Correlation of annual ACE and JAS Niño3.4 index	--	0.06	0.13	**0.40***	**0.40***
Correlation of annual NTC and JAS PDO index	-0.05	0.09	-0.01	**0.41***	**0.26**
Correlation of annual ACE and JAS PDO index	--	0.08	0.10	**0.40***	**0.40***

561 **Table 2** Various features of every cluster and all MHs during 1970-2018 in ENP. Percent values

562 represent the proportions within each cluster. One ACE equals to 10000 kt^2 (kn^2).

Features of MHs	Cluster A	Cluster B	Cluster C	All MHs
Major activity month	Jul-Aug	Jul-Sep	Jun-Oct	Jun-Sep
Median genesis location	233.6°E, 11.0°N	253.5°E, 11.5°N	260.6°E, 12.0°N	257.2°E, 11.9°N
Activity Regain	182.7-227.5°E 11.8-23.6°N	213.4-245.0°E 13.4-19.5°N	240.4-256.0°E 13.4-21.2°N	--
Mean duration per storm (day/d)	8-16	8-13	7-10	7-11
Landfalling rate (percentage)	5%	2%	31%	18%
Mean translation speed (km/h)	18.77	19.32	14.88	17.07
Mean NMH per year	0.80	1.29	2.46	4.55
Mean ACE per year	19.10	28.29	44.67	92.06
Mean ACE per MH	23.88	21.93	18.16	20.23

563

564

565 **Figures**

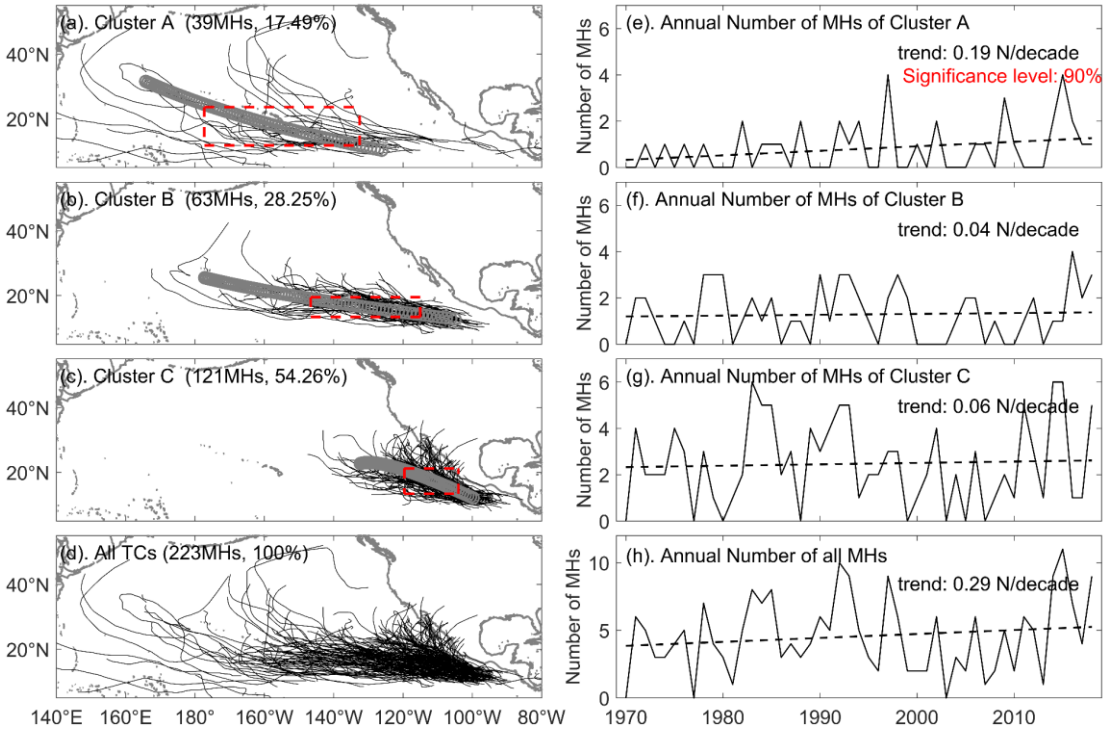

566

567 **Fig. 1** (**a-d**) MH tracks (black lines) of three clusters and all MHs during 1970-2018 in ENP, and

568 each cluster's mean regression curve is marked in gray open circles. Each cluster's main activity

569 region is shown in red dashed box. The title of each sub-graph shows the name of cluster or all MHs,

570 follow the number of MHs and their percentage within all MHs in parentheses. (**e-h**) Annual number

571 of MHs of three clusters and all MHs, and their linear trends.

572

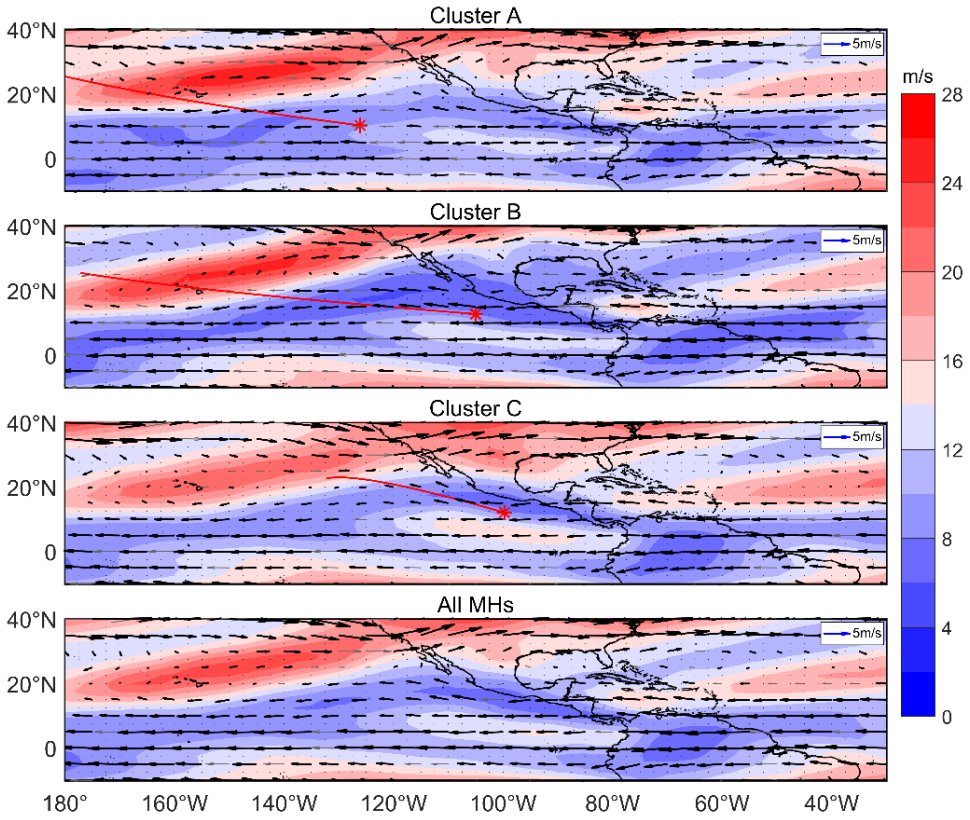

573

574 **Fig. 2** Composites of steering flow (SF) (vector; m/s) and VWS (shading; m/s) for MHs in each

575 cluster and all MHs during 1970-2018 in ENP. The composites are calculated on whole active days of

576 MHs. We mark the 95% significant areas in black arrows and dots. Besides, each cluster's mean

577 regression curve is shown in red line (trajectory) and asterisk (generation location).

578

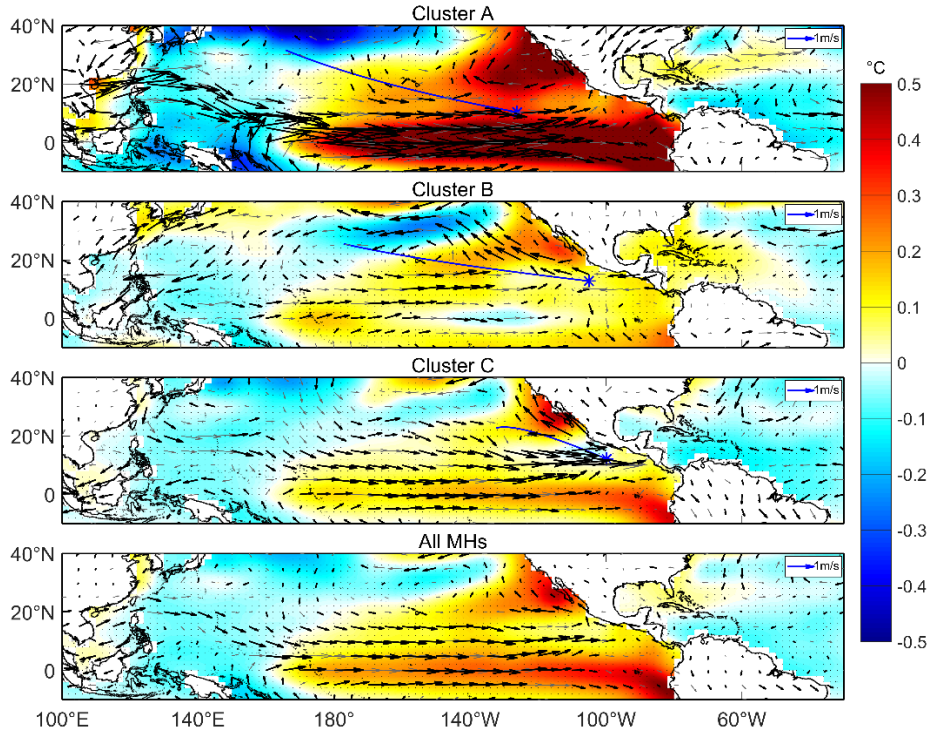

Fig. 3 As in **Fig. 2**, but for composites of SST anomaly (shading; °C) and wind anomaly at 850-hPa (vector; m/s). Besides, each cluster's mean regression curve is shown in blue line (trajectory) and asterisk (generation location).

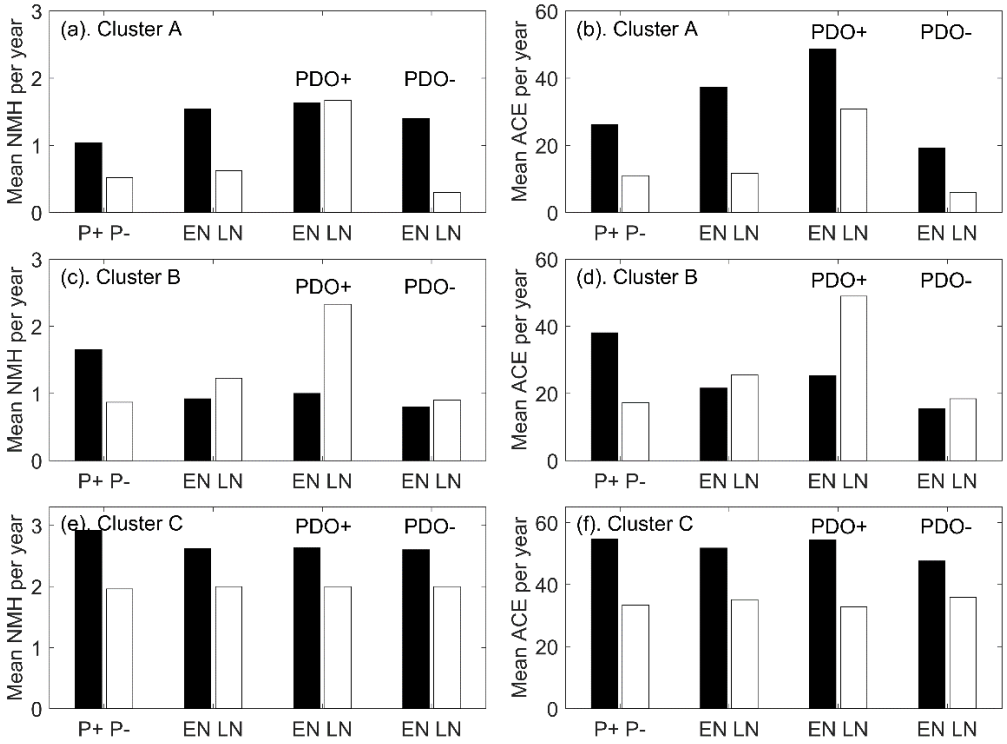

584

585 **Fig 4** Mean NMH (**a**, **c** and **e**) and ACE (**b**, **d** and **f**) per year of each cluster in different PDO and

586 ENSO years, "+" describes positive (warm) phase and "-" describes negative (cold) phase, "P"

587 describes PDO, "EN" describes El Niño and "LN" describes La Niña. One ACE equals to 10000 kt^2

588 (kn^2).

589

590

591

592

593

594

595

596

597

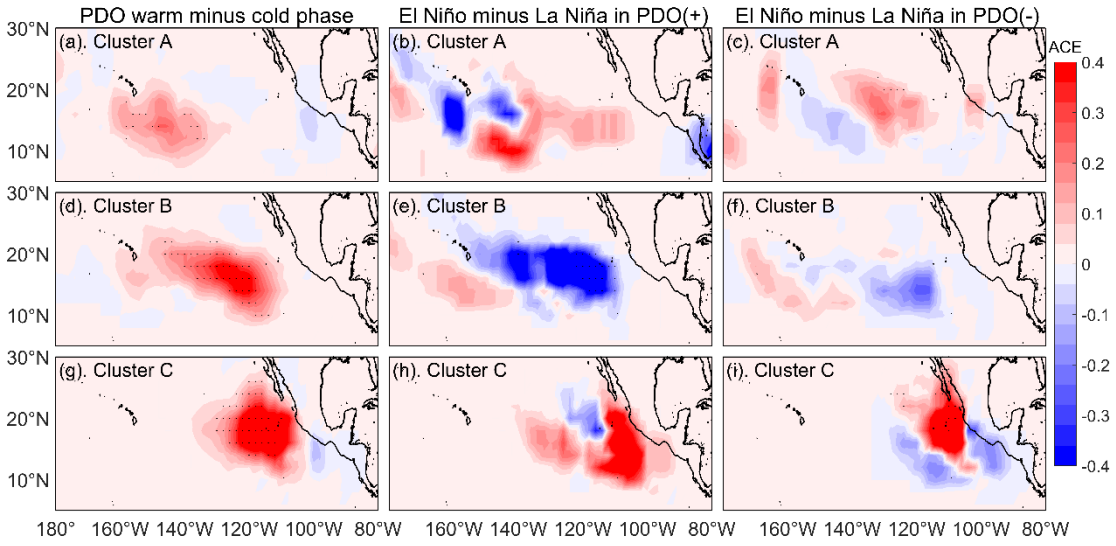

598

599 **Fig. 5** Composite differences of ACE between PDO warm and cold phase (left column), composite

600 differences of ACE between El Niño and La Niña in the PDO warm phase (middle column) and cold

601 phase (right column) of cluster A (**a**, **b**, **c**), cluster B (**d**, **e**, **f**) and cluster C (**g**, **h**, **i**). One ACE equals to

602 10000 kt^2 (kn^2). We mark the 95% significant areas in black dots.

603

604

605

606

607

608

609

610

611

612

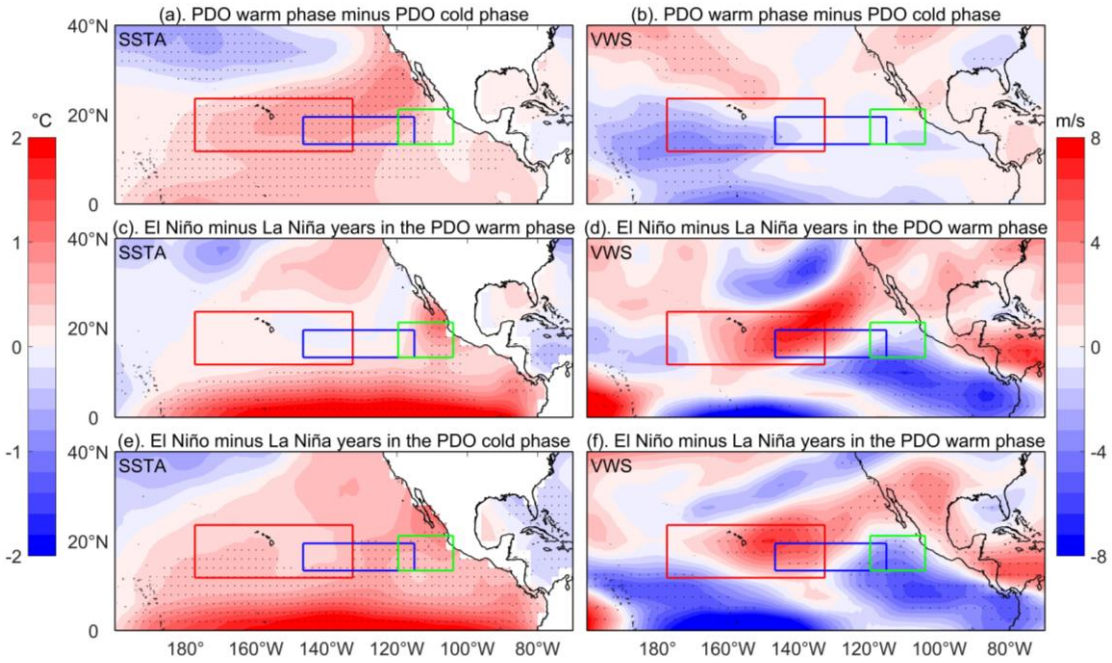

Fig. 6 Composite differences of (**a**, **c**, **e**) SSTA and (**b**, **d**, **f**) VWS in averaged JAS between the PDO warm and cold phase (**a**, **b**), between El Niño and La Niña years in the PDO warm phase (**c**, **d**) and PDO cold phase (**e**, **f**). We mark the 95% significant areas in black arrows and dots, each cluster's main activity region is shown in red (bule and green) solid box for cluster A (B and C).

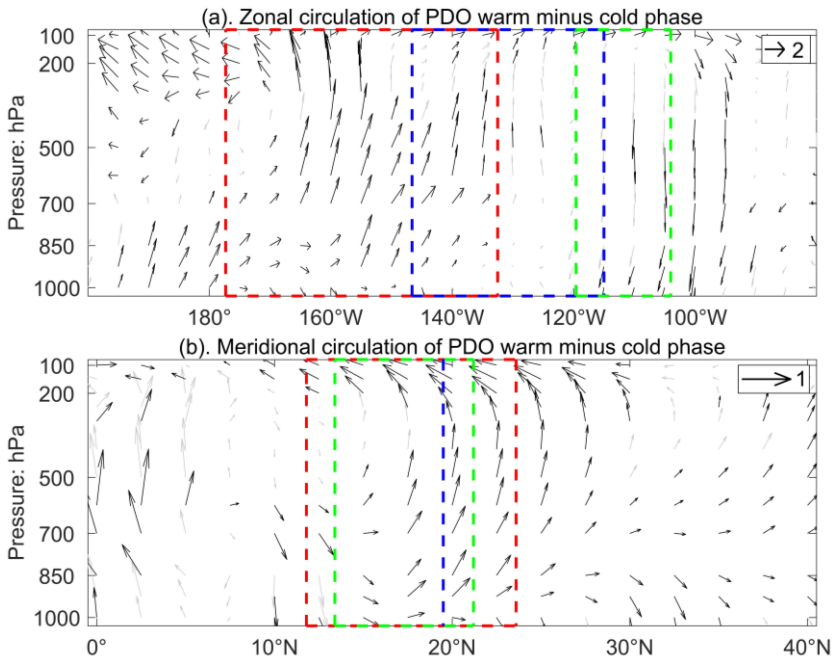

627

628 **Fig. 7** (**a**) Composite differences of zonal circulation which averaged in latitude range of main

629 activity region of three clusters between the PDO warm and cold phase. (**b**) Composite differences of

630 meridional circulation which averaged in longitude range of main activity region of three clusters

631 between the PDO warm and cold phase. We mark the 95% significant areas in black arrows. Each

632 cluster's main activity region is shown in red (bule and green) dashed box for cluster A (B and C). The

633 unit of zonal winds is m/s, the vertical velocity is taken to be the negative of the pressure vertical

634 velocity and its unit is 10^2 Pa/s.

635

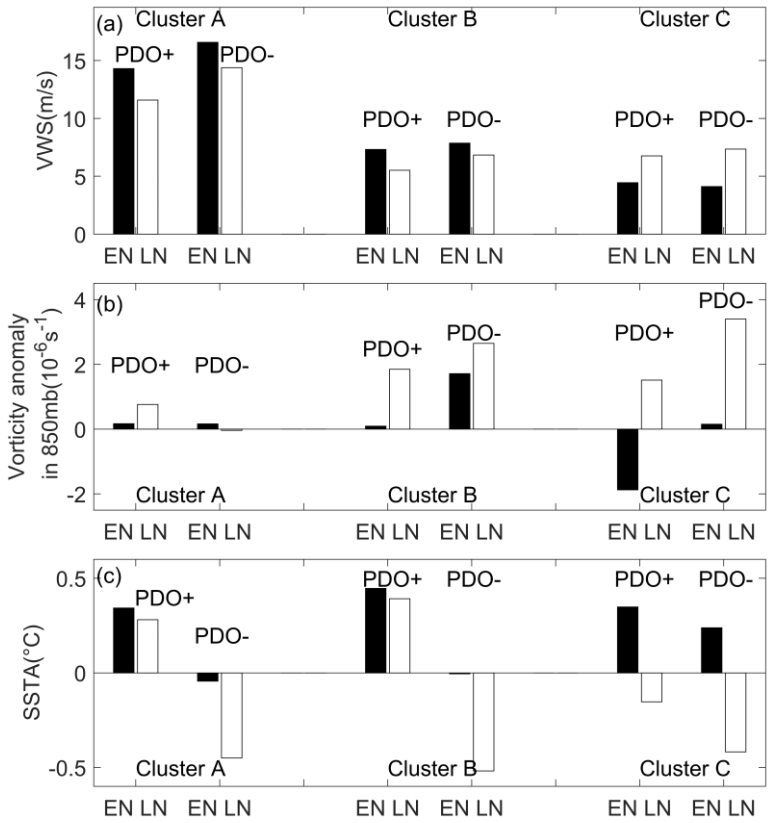

Fig. 8 Mean vertical wind shear (**a**), vorticity anomaly in 850mb (**b**) and SST anomaly (**c**) in averaged JAS per year in the main activity region of each cluster in different ENSO and PDO phases years. "+" describes positive phase and "-" describes negative phase, "P" describes PDO, "EN" describes El Niño and "LN" describes La Niña, also for the next figures.

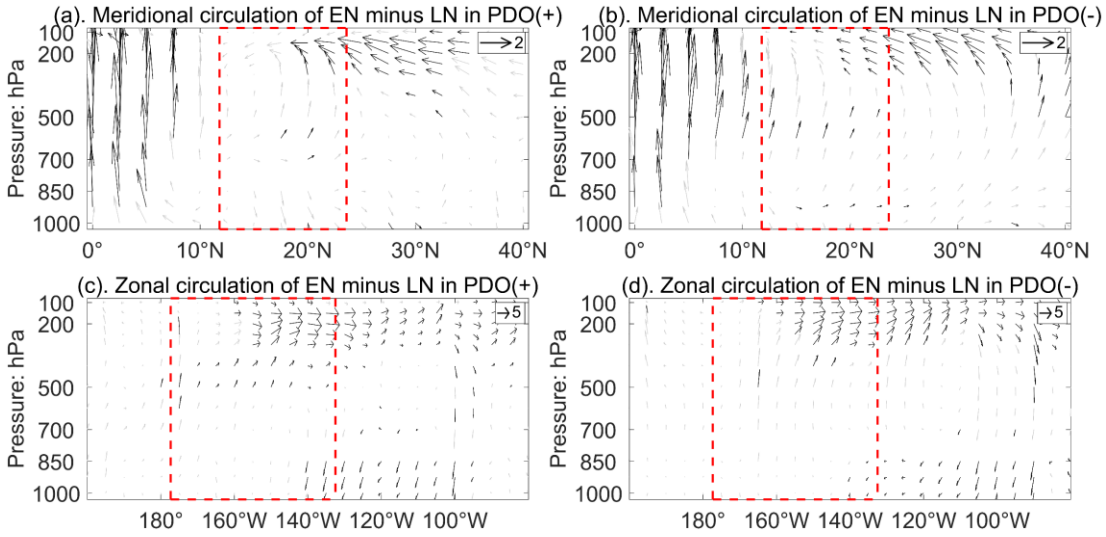

643

644 **Fig. 9** Composite differences of meridional circulation which averaged in longitude range of main

645 activity region of cluster A between El Niño and La Niña years in the PDO warm (**a**) and PDO cold

646 (**b**) phase. Composite differences of zonal circulation which averaged in latitude range of main

647 activity region of cluster A between El Niño and La Niña years in the PDO warm phase (**c**) and PDO

648 cold phase (**d**). We mark the 95% significant areas in black arrows. The main activity region of cluster

649 A is shown in red dashed box. The unit of zonal winds is m/s, the vertical velocity is taken to be the

650 negative of the pressure vertical velocity and its unit is 10^2 Pa/s.

651

652

653

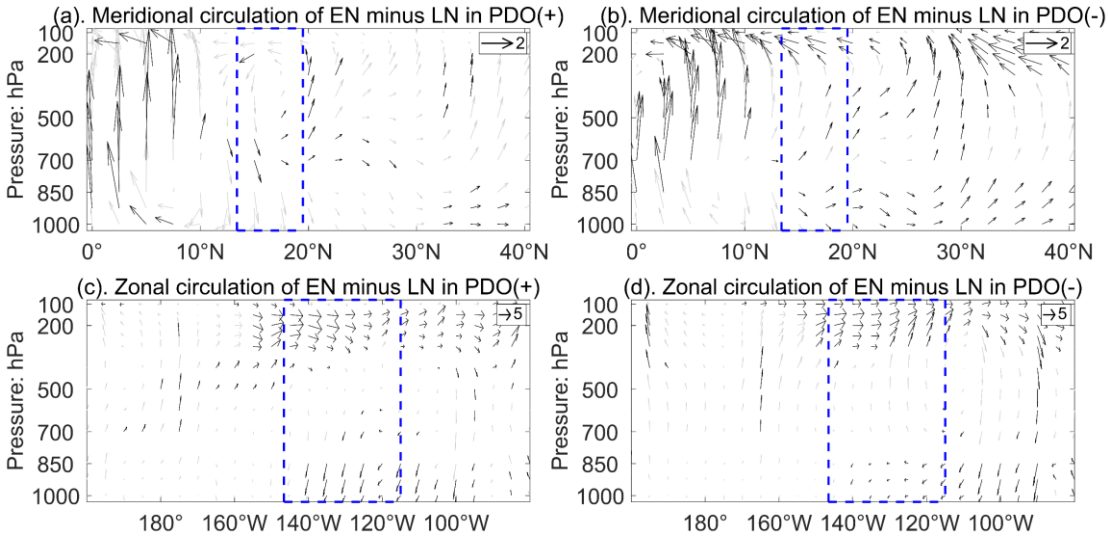

654

655 **Fig. 10** As in **Fig. 9**, but for composite differences of meridional circulation (**a**, **b**) and zonal

656 circulation (**c**, **d**) for cluster B.

657

658

659

660

661

662

663

664

665

666

667

668

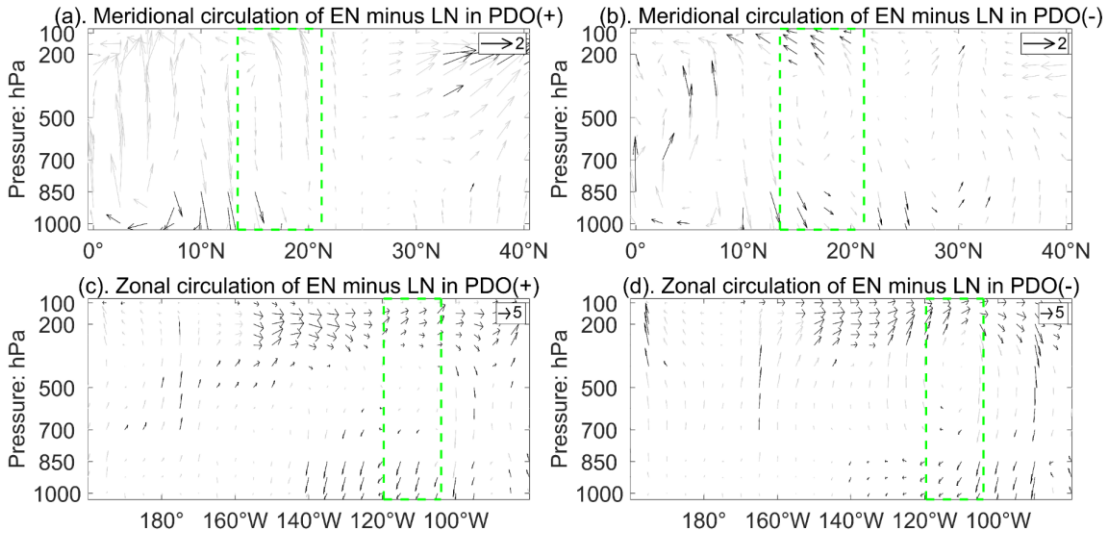

669

670 **Fig. 11** As in **Fig. 9**, but for composite differences of meridional circulation (**a**, **b**) and zonal

671 circulation (**c**, **d**) for cluster C.

672

673

674

675

676

677

678

679

680

681

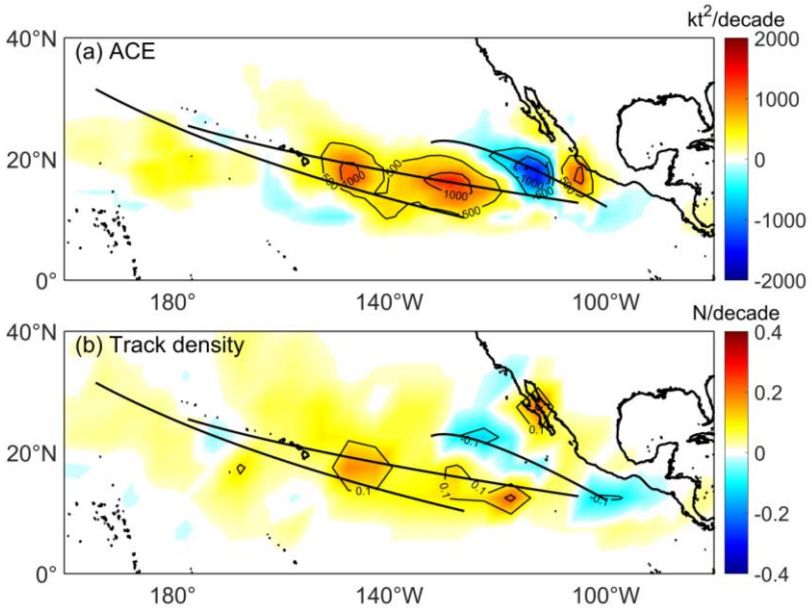

682

683 **Fig. 12** Trend distribution of (a) ACE and (b) track density of MHs in 1970-2018. The mean

684 regression curves of three clusters are shown in black solid lines.

685

686

687

688

689

690

691

692

693

694

695

696

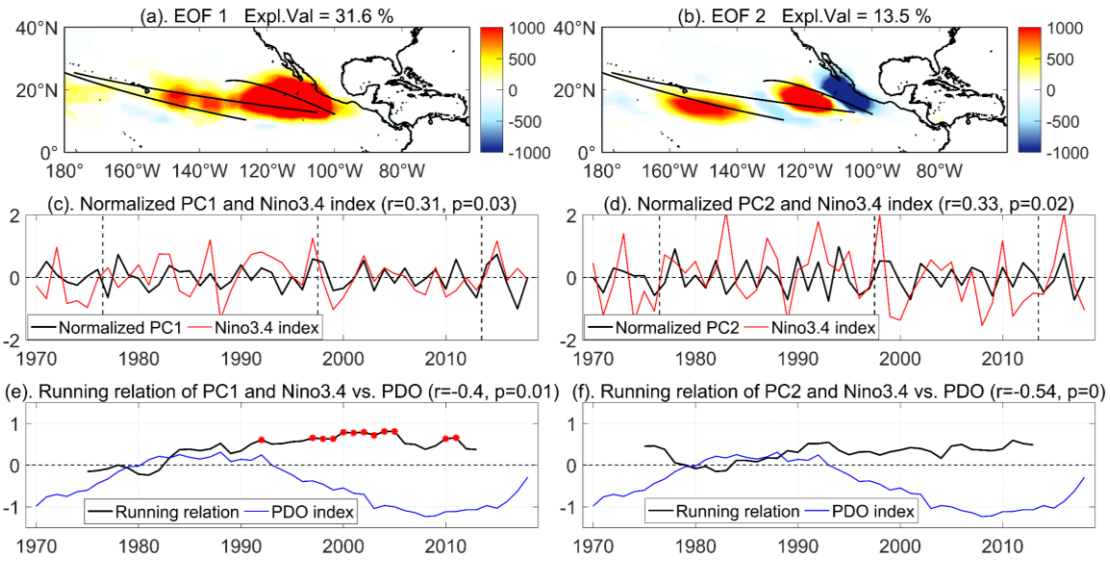

Fig. 13 First two modes of EOF analysis for MHs ACE that 2-7 years pass filtered. (**a**, **b**) is spatial mode, the mean regression curves of three clusters are shown in black solid lines. (**c**, **d**) is the normalized PC time series (black line) and Niño3.4 index (red line). (**e**, **f**) is 10-year sliding correlation between normalized PC and Niño3.4 index during 1970-2018 (black line, red asterisks that indicate 95% confidence level), and PDO index (blue line) which calculated by 11 years running mean. Nino3.4 index is averaged in May-Jul for PC1 and Jan-Mar for PC2.

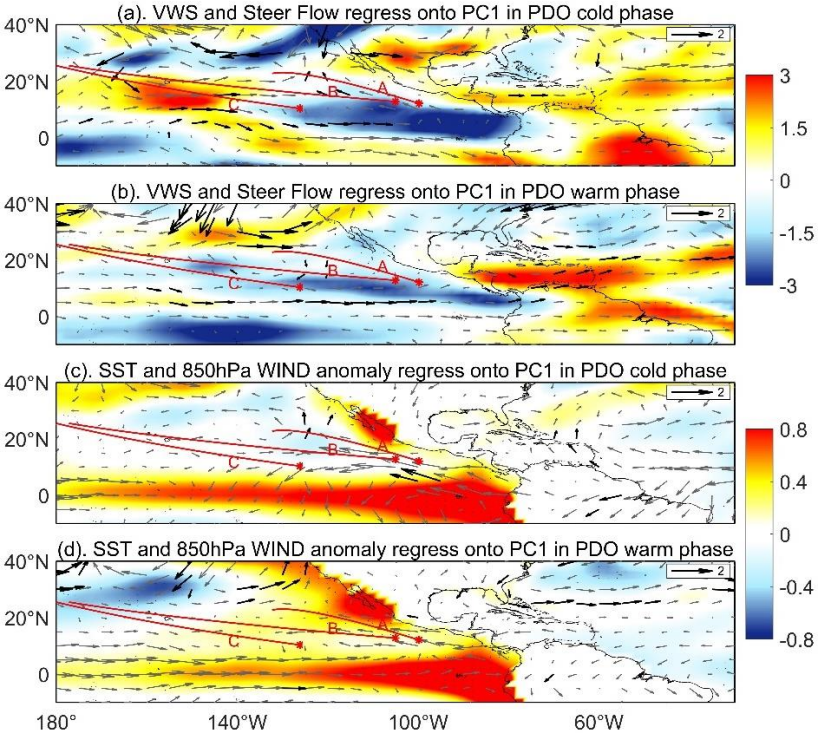

705

706 **Fig. 14** Regression of (**a**, **b**) VWS (shading; m/s) and SF (vector; m/s), (**c**, **d**) SST (shading; °C)

707 and 850-hPa wind (vector; m/s) anomaly regression onto normalized PC1 in the PDO cold phase (**a**, **c**)

708 and warm phase (**b**, **d**). Stippling indicates linear correlation coefficient at the 95% significance level

709 for SST anomaly and VWS. And black arrows for SF and 850-hPa wind anomaly with the linear

710 correlation coefficient at a 0.05 significance level. SST anomaly were averaged in May-Jul, other

711 environmental variables were averaged in July to September (JAS). The mean regression curves of

712 three clusters are shown in red solid lines.

713

714

715

716

717

718

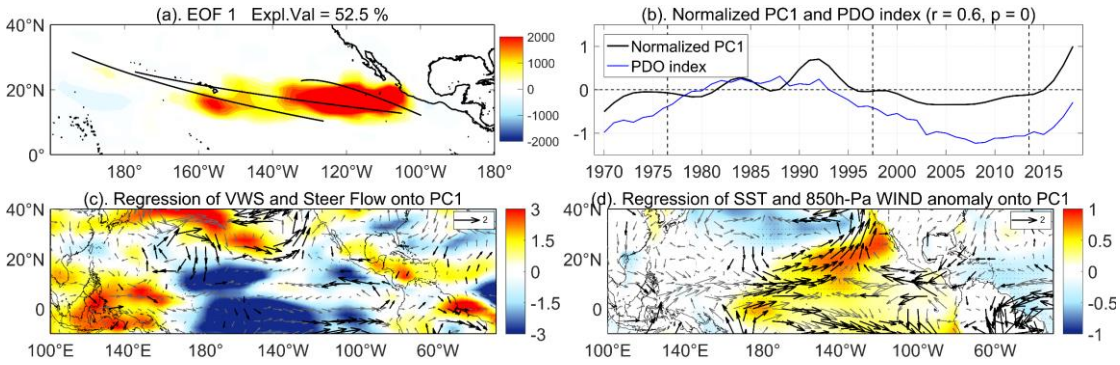

719

720 **Fig. 15** First mode of EOF analysis for MHs ACE that longer 7 years pass filtered. (**a**) is the spatial

721 mode, the mean regression curves of three clusters are shown in black solid lines. (**b**) is normalized

722 PC time series (black line) and PDO index (blue line) which calculated by 11 years running mean. (**c**,

723 **d**) VWS (shading; m/s) and SF (vector; m/s), SST anomaly (shading; °C) and 850-hPa wind anomaly

724 (vector; m/s) regression onto normalized PC1. Stippling indicates linear correlation coefficient at a

725 0.05 significance level for SST anomaly and VWS. And black arrows for SF and 850-hPa wind

726 anomaly with the linear correlation coefficient at a 0.05 significance level.

727